2018

Is AlOH the Astrochemical Reservoir Molecule of AlO?: Insights from Excited Electronic States

Tarek Trabelsi
University of Nebraska - Lincoln

Joseph S. Francisco
University of Nebraska - Lincoln, frjoseph@sas.upenn.edu

The Astrophysical Journal, 863:139 (6pp), 2018 August 20 https://doi.org/10.3847/1538-4357/aad5e0

Is AlOH the Astrochemical Reservoir Molecule of AlO?: Insights from Excited Electronic States

Tarek Trabelsi and Joseph S. Francisco
Department of Chemistry, University of Nebraska-Lincoln, Lincoln, NE 68588, USA; jfrancisco3@unl.edu
Received 2018 May 25; revised 2018 July 19; accepted 2018 July 19; published 2018 August 20

Abstract

Very recently, the optical bands of the $^2\Sigma^+ \leftarrow X^2\Sigma^+$system of AlO have been identified in the red supergiant star VYCMa. In an effort to explain the origin of this transition, we used state-of-the-art quantum chemical calculations with proven high accuracy to compute the lowest singlet and triplet electronic states of the AlOH and HAlO isomers as well as their equilibrium geometry and electronic properties. Our calculated potential energy surfaces implicate the three singlet electronic states $2^1A'$, $3^1A'$, and $1^1A''$ in the photodissociation of the [Al,O,H] system. Only AlO, H, Al, and OH products can occur through the photodissociation of [Al,O,H]; AlH and O are not allowed. For the photodissociation of AlOH, the AlO product can occur only in its excited states AlO($^2\Pi$) and AlO($^2\Sigma^+$).

Key words: astrochemistry – supergiants – techniques: spectroscopic – ultraviolet: ISM

1. Introduction

Metal-containing molecules have received increased attention in the recent years as an increasing number of systems have been detected in the interstellar medium (ISM). Metal-containing species detected in the ISM include AlNC (Ziurys et al. 2001), MgCN (Ziurys et al. 1995), KCN (Pulliam et al. Pulliam et al. 2010), AlO (Tenenbaum & Ziurys 2009), and AlOH (Tenenbaum & Ziurys 2010). Among the aluminum-bearing molecules, the diatomic AlO has been detected in the circumstellar shell of red supergiant star VYCMa (Tenenbaum & Ziurys 2009), with an observed abundance of $6 \cdot 10^{-9}$. Its formation mechanism is associated with the gas-phase local thermodynamic equilibrium (LTE) chemistry. Recently, Kamiński et al. (2013) confirmed the existence of AlO; specifically, they observed the $B^2\Sigma^+$–$X^2\Sigma^+$ electronic transition and suggested several mechanisms to explain its origin. Both the millimeter-wave and optical spectrum detection of AlO gas suggest its existence at ∼20 stellar radii. This result contradicts the LTE model, which predicts substantial AlO abundances to within only a few stellar radii. In 2010, aluminum monohydroxide (AlOH), the most stable isomer of HAlO, was detected in the envelop of VYCMa (Tenenbaum & Ziurys 2010), with an observed abundance of $1 \cdot 10^{-7}$, which is relatively higher than the abundance of AlO and closer to the abundance of aluminum ($3 \cdot 10^{-6}$). Its formation has been suggested to occur by LTE chemistry. LTE calculations predict that AlOH is the most abundant aluminum-bearing molecule in the 2–8 stellar radii region (Tenenbaum & Ziurys 2009). Hydrogen is well known to be the most abundant element in the ISM, and AlO and AlOH have been detected in the envelope of VYCMa; however, the simplest diatomic aluminum molecule, AlH, has not yet been detected in the VYCMa star, which is somewhat surprising. The reasons for this non-detection are unclear.

The circumstellar envelope of red supergiant stars such as IRC+10216 and VYCMa foster gas-phase chemistry (McCabe et al. 1979; Ziurys 2006; Parsons et al. 2010). In these stars, a photochemistry process induced by UV-Vis photons can play an important role in both the formation and the destruction of molecular species. Generally, daughter molecules originate from the photodissociation of parent molecules. For instance, OH and O_2 are the most abundant oxygen-bearing daughter species triggered by the chemistry of water (Li et al. 2016). Although the electronic structures, spectral features, and isomerization processes of AlOH and HAlO isomers are well known, knowledge of their photochemistries is still lacking. Pilgrim et al. (1993) reported the electronic spectrum for AlOH formed in a laser-vaporization pulsed molecular beam source. They observed two electronic states spaced by 1674 cm^{-1}. The authors could not unambiguously assign these states to either the AlOH or the HAlO isomer. Li et al. (2003) conducted theoretical calculations to characterize the three lowest-lying singlet states of AlOH using several levels of theory.

Little is known about the electronic spectroscopy and photochemistry of the [Al, O, H] molecular system. In this work, we focus on the photochemical and photophysical processes of AlOH and HAlO isomers. The answers to some fundamental questions in photochemistry may explain the non-detection of AlH in VYCMa and reveal which products are favored after the photodissociation of AlOH and HAlO isomers. However, investigations of the lowest singlet and triplet electronic states can answer the question of whether AlO is the daughter molecule of AlOH.

2. Theoretical Background

All calculations were carried out with the MOLPRO2015 program (Werner 2015). The starting points of this work were the electronic structures and vertical excitation energies to the low-lying singlet and triplet electronic states. The search of the stationary points of AlOH and HAlO were performed at the explicitly coupled cluster theory RCCSD(T)-F12 (Adler et al. 2007; Werner et al. 2007; Knizia et al. 2009) in conjunction with large basis sets aug-cc-pV5Z. As shown in previous work (Hauge et al. 1980), the ground electronic state of AlOH is flat and quasilinear, and explicit treatment of the electron correlation is needed (Kalugina et al. 2014). For both isomers, optimized equilibrium geometries were carried out in the C_1 symmetry group. To investigate the lowest electronic states, we used the complete active space self-consistent field (CASSCF; Knowles & Werner 1985; Werner & Knowles

Table 1
Optimized Equilibrium Geometry (Distance in Å and θ in Degrees), Harmonic Vibration Frequencies (ω in cm^{-1}), and Relative Energy of AlOH and HAlO Isomers in Their Ground Electronic States

	R_{AlO}	R_{OH}	θ	ω_1	ω_2	ω_3	Er/eV
AlOH(X^1A')							
CCSD(T)-F12/aug-cc-pV5Z	1.6804	0.9497	161.0	4009.9	129.4	845.7	0.0
CCSD(T)/aug-cc-pV5Z	1.6823	0.9499	160.9	4009.1	133.3	843.3	0.0
MRCI-F12/aug-cc-pV5Z	1.7084	0.9424	134.2	4183.9	485.9	806.8	0.0
MRCI+Q/aug-cc-pV5Z	1.7021	0.9441	139.0	4129.5	380.0	809.8	0.0
expt[a]				3790		810.3	
expt[b]						895	
	R_{AlO}	R_{AlH}	θ	ω_1	ω_2	ω_3	Er/eV
HAlO($X^1\Sigma^+$)							
CCSD(T)-F12/aug-cc-pV5Z	1.6036	1.5649	180.0	2014.2	418.0	1067.9	1.74
CCSD(T)/aug-cc-pV5Z	1.6054	1.5651	180.0	2012.5	418.5	1064.9	1.74
MRCI-F12/aug-cc-pV5Z	1.6001	1.5551	180.0	2101.9	461.3	1077.6	1.49
MRCI+Q/aug-cc-pV5Z	1.6051	1.5563	180.0	2097.5	456.4	1076.7	1.54

Notes.
[a] Reference: Pilgrim et al. (1993).
[b] Reference: Hauge et al. (1980).

1985) followed by the internally contracted multireference configuration interaction (MRCI; Knowles & Werner 1988; Werner & Knowles 1988) methods, as implemented in the MOLPRO package. In MRCI/CASSCF calculations, all the valence orbitals were employed without any restriction. In these calculations, the atoms were described by the aug-cc-pV5Z basis sets. Our interest was in the dissociation of AlOH and HAlO isomers along the Al–O, O–H, and H–Al stretches. Evolution of the lowest electronic state along the bending angle were also mapped. To consider all the states involved in the photodissociation process, all singlet and triplet electronic states that correlated to the first three dissociation limits of AlO+H, the first two dissociation limits of AlH+O and one dissociation limit of Al+OH, were calculated. Because of the non-size consistency of the MRCI method, the Davidson correction (Langhoff & Davidson 1974) was used to obtain an accurate value of the dissociation limits and the equilibrium geometries of the lowest electronic states. From the CASSCF wavefunction, the transition dipole moment was evaluated to calculate the lifetime (τ, in s), which is related to the square of the transition dipole moment ($|R_{e,i}|^2$, in Debye) via the equation

$$\tau_n(s) = 6.07706 \times 10^{-6} \sum_i^n \frac{1}{|R_{e,i}|^2\ \delta E_i^3}, \quad (1)$$

where δE_i is the energy transition in eV and n is the number of electronic states.

3. Results and Discussion

3.1. Electronic Ground States of AlOH and HAlO

The optimized equilibrium geometries of AlOH and HAlO isomers in their ground electronic states are listed in Table 1. All levels of theory suggested that AlOH is the most stable isomer, with Al–O and O–H bond lengths of 1.702 and 0.944 Å, respectively, at the MRCI+Q level of theory. Table 1 shows no coherence between the equilibrium geometries of AlOH calculated at the MRCI and the CCSD(T) levels of theory. Multireference and explicitly multireference treatment of the electron correlation at the MRCI+Q and MRCI-F12 levels, respectively, in conjunction with the large basis sets aug-cc-pV5Z showed that the global minimum was located at $\theta \approx 134°$, whereas an explicit treatment of the electron correlation at the CCSD(T)-F12 level showed that the global minimum was located at $\theta = 161°$. All levels of theory showed a real minimum on the potential energy surface because all their harmonic vibrational frequencies were positives.

The AlOH molecule is quasilinear in its ground electronic state, meaning that, along the bending angle, the potential energy surface will be too flat with small harmonic vibrational frequencies. For the bending mode, we calculated the harmonic vibrational frequency at the MRCI+Q level to be $\omega_2 = 380\,cm^{-1}$ and that at the MRCI-F12 level to be $\omega_2 = 485\,cm^{-1}$. These values are relatively large and cannot describe a flat potential. At the CCSD(T)-F12 level, the barrier to linearity was calculated at $5.3\,cm^{-1}$, confirming that AlOH is quasilinear, with small bending frequencies calculated at $129.4\,cm^{-1}$. The results obtained with both methods, CCSD(T) and CCSD(T)-F12, are in good agreement with previous work (Li et al. 2003) which showed that the bending angle of AlOH in its ground electronic state is 160°.

The predicted harmonic vibrational frequency ω_1 for AlOH is in good agreement with previous theoretical work (Li et al. 2003) and relatively far compared to the experimental work of Pilgrim et al. (1993). In fact, in the diatomic OH, the experimental values of the harmonic vibrational frequencies and the OH bond length (Mizushima 1972) are $\omega(OH) = 3737\,cm^{-1}$ and $rOH = 0.969$ Å, respectively. Optimized equilibrium geometry at CCSD(T) and CCSD(T)-F12 levels show that the equilibrium distance of OH decreased by 0.02 Å, meaning that the harmonic stretch (OH) should increase.

For the HAlO($X^1\Sigma^+$) isomer, which is 1.74 eV higher in energy than AlOH, CCSD(T) and MRCI were in good agreement. At the MRCI-F12 level of theory, the AlO bond length was predicted to be $R_{AlO} = 1.6036$ Å and $R_{AlO} = 1.6804$ Å in the AlOH isomer. The equilibrium bond length for the diatomic AlO($X^2\Sigma^+$) was determined to be $R_{AlO} = 1.620$ Å at the same level. Therefore, the AlO distance of AlOH was predicted to be longer than in AlO($X^2\Sigma^+$) and HAlO, which is in agreement with the AlO stretch (ω_3) that is decreased relative to its value in AlO ($994.1\,cm^{-1}$; Sghaier et al. 2016) and HAlO ($1077.6\,cm^{-1}$). Here, we were interested in the electronic spectroscopy and the stability

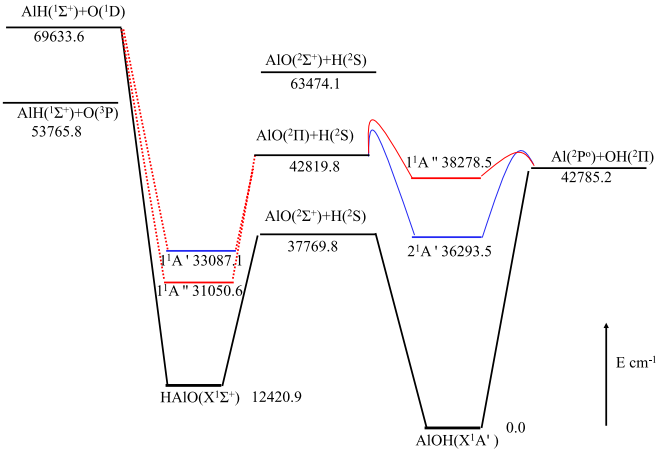

Figure 1. MRCI+Q/aug-cc-pV5Z adiabatic energetic diagram of the lowest dissociation limits of the AlOH and HAlO systems. The reference energy is the energy of AlOH(X^1A') including zero-point vibrational correction.

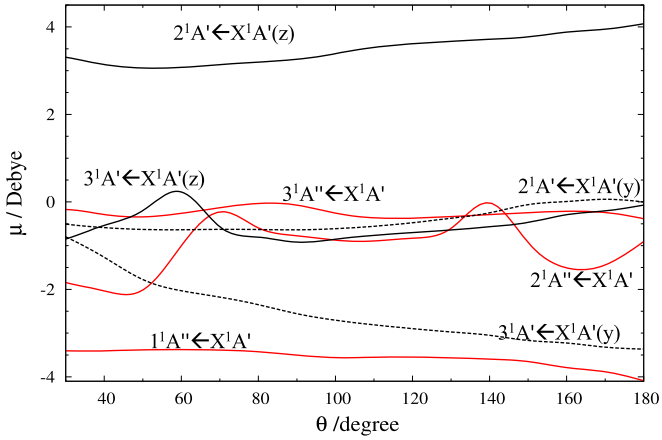

Figure 2. One-dimensional cut of the evolution of the transition dipole moment from the ground state of AlOH(X^1A') to $2^1A'$, $3^1A'$, $1^1A''$, $2^1A''$, and $3^1A''$ electronic states along the bending angle. The y and z components of the transition moments are planted separately.

Table 2
MRCI+Q/aug-cc-pV5Z Optimized Equilibrium Geometry (Distance in Å and θ in Degrees), Harmonic Vibration Frequencies (ω_i in cm^{-1}), and Vertical (T_e in eV) and Adiabatic (T_0 in eV) Excitation Energy of the Lowest Electronic States of AlOH and HAlO

AlOH											
States		R_{AlO}	R_{OH}	θ	ω_1	ω_2	ω_3	T_e	T_0	$\lvert\mu\rvert_{A\leftarrow X}$	τ (ns)
X $^1A'$		1.702	0.944	139.0	4129.5	380.0	809.8	0.00	0.00		
1 $^3A'$		1.717	0.961	117.1	3841.9	674.7	824.2	3.37	2.67		
1 $^3A''$		1.702	0.952	130.7	3969.4	448.2	839.4	3.46	2.80		
2 $^1A'$		1.755	0.963	110.1	3834.2	657.8	843.5	5.54	4.50	4.25	1.97
1 $^1A''$		1.741	0.960	116.7	3854.6	575.7	780.3	5.59	4.73	4.26	1.91
					HAlO						
States		R_{AlO}	R_{HAl}	θ	ω_1	ω_2	ω_3	T_e	T_0	$\lvert\mu\rvert_{A\leftarrow X}$	τ (ns)
X $^1\Sigma^+$	X^1A'	1.601	1.556	180.0	2086.0	452.0	1069.1	0.0	0.00		
$^3\Pi$	$^3A'$	1.726	1.610	94.7	1827.9	808.5	948.3	3.79	2.19		
	$^3A''$	1.780	1.602	116.9	1827.8	582.6	735.5		2.22		
$^1\Pi$	$^1A''$	1.772	1.599	116.5	1835.9	596.0	748.4	4.07	2.29		
	$^1A'$	1.743	1.609	119.4	1792.6	568.4	809.1		2.54	1.87	25.7
$^3\Sigma^+$	$^3A'$							4.08			

Note. Also given are the transition dipole moment ($\lvert\mu\rvert_{A\leftarrow X}$ in debye) and the lifetime (τ in ns) of the lowest singlet states.

of the lowest electronic state of both the AlOH and the HAlO isomer. In the following section, we use the CCSD(T)-F12/aug-cc-pV5Z optimized equilibrium geometries to describe the behavior of the lowest electronic states.

3.2. Potential Energy Surfaces

We started our investigations by exploring the topology of the potential energy surfaces (PESs) of the low-lying singlet and triplet electronic states for linear AlOH (i.e., $C_{\infty v}$ point group) and bent HAlO isomer (i.e., C_s point group). Figure 1 displays the energetic diagram of AlOH and HAlO calculated at the MRCI+Q/aug-cc-pV5Z level of theory. The adiabatic electronic excitation energies of AlO were taken from Michels (1972) and Rosenwaks et al. (1975). This diagram was corrected at the zero-point energy (ZPE), and the origin of energy is the energy of AlOH in its ground electronic state (X^1A'). The optimized equilibrium geometry of the lowest singlet and triplet states, as well as the vertical and adiabatic excitation energies and transition dipole moment, are listed in Table 2.

Figure 2 shows the evolution of the transition dipole moment along the bending angle. Figure 3 displays one-dimensional cuts of the lowest electronic states of the bent AlOH isomer along the AlO (Figure 3(a)) and OH (Figure 3(b)) bond lengths to approximately 8 eV above the ground-state minimum. The other coordinates were fixed to their equilibrium values.

Figure 4 shows the evolution of the PESs along the bending angle. Their correlations at linearity were made explicit by the corresponding spectroscopic term placed at the right-hand side of the figure. Figure 3 shows that the first two triplet states, $1^3A'$ and $1^3A''$, are stable with respect to dissociation, their minimum is located below the first dissociation limit, and they have a potential well. These two states were located at 2.67 eV for $1^3A'$ and at 2.80 eV for $1^3A''$, respectively, above the global minimum of AlOH. Along the bending angle, several exited states showed a flat potential and were coupled by Renner–Teller coupling (Figure 4(a)). For instance, the $1^3A'$ and $1^3A''$ states correlated to the $^3\Pi$ state at linearity. The optimized geometries of these two triplet states predicted a larger OH bond length than the OH bond length of the ground state (Table 2). The first lowest singlet states $2^1A'$ and $1^1A''$ showed a shallow potential along the AlO and OH coordinates.

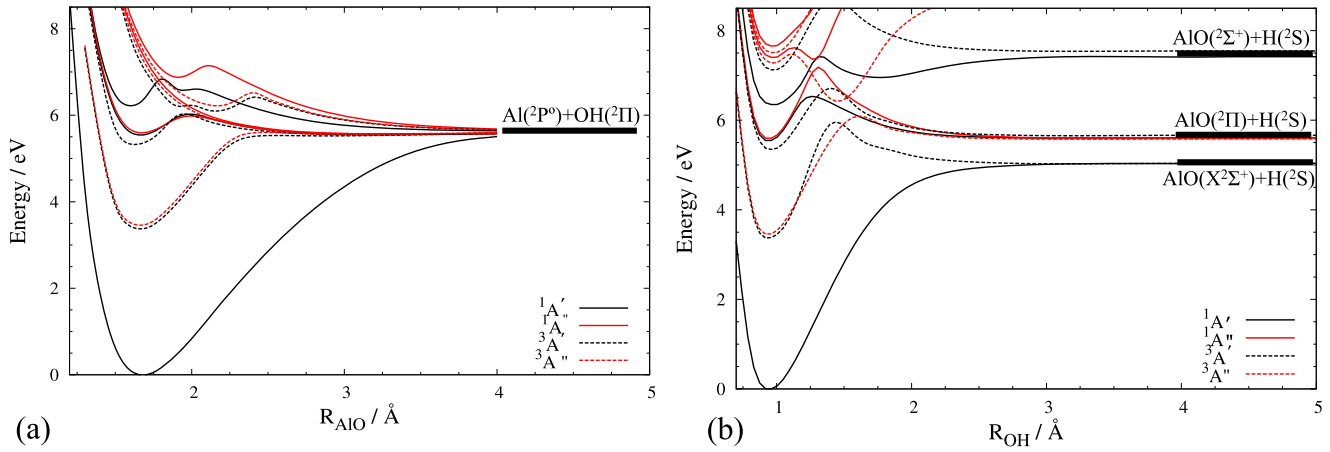

Figure 3. MRCI/aug-cc-pV5Z one-dimensional cut of the lowest singlet and triplet electronic states of AlOH along the R_{AlO} (a) and R_{OH} (b) distances. The remaining coordinates were kept fixed at their equilibrium values.

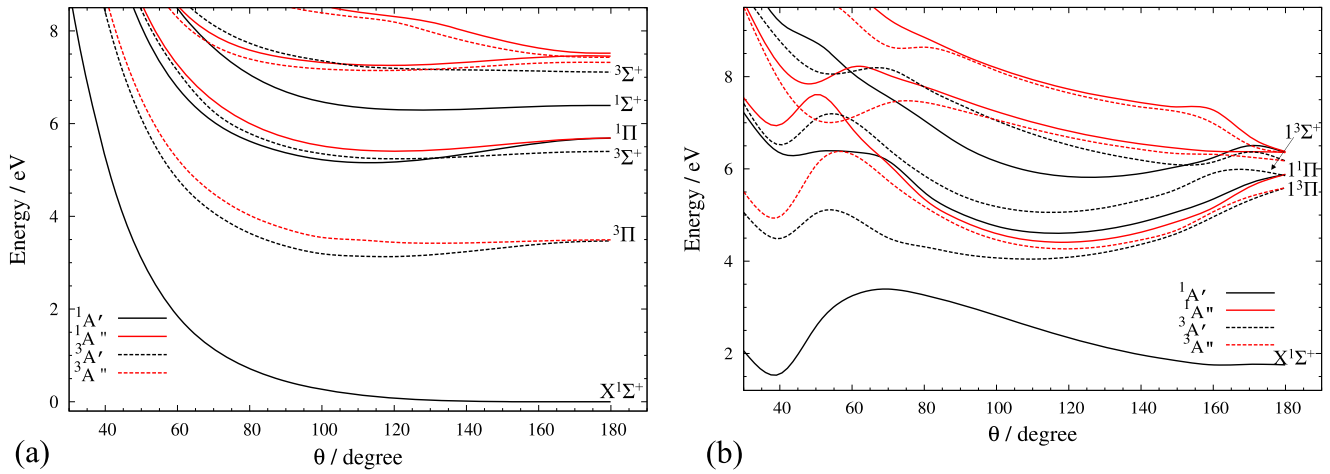

Figure 4. MRCI/aug-cc-pV5Z one-dimensional cut of the lowest singlet and triplet electronic states of AlOH (a) and HAlO (b) along the bending angle. The remaining coordinates were kept fixed at their equilibrium values. The origin of energy was the energy of AlOH in its ground electronic state.

These two electronic states, $2^1A'$ and $1^1A''$, correlate to a $^1\Pi$ state at linearity and are coupled by Renner–Teller coupling.

Both the $2^1A'$ and the $1^1A''$ potential energies exhibited several avoided crossings. Because of the limited number of states calculated, some avoiding crossing at energies above 7.5 eV were not fully resolved. The relatively flat potential around $R_{OH} = 1.75$ Å in Figure 3(b) is the result of avoidance with the next-higher $4^1A'$ state. These avoided crossings between the electronic state with the same spin symmetry should favor mixing of their wavefunctions and complicate their electronic and rovibrational spectra. Furthermore, they play an important role in the photodissociation process. At the MRCI+Q/aug-cc-pV5Z level of theory, we calculated the adiabatic excitation energy from the ground state to the $2^1A'$ and $1^1A''$ electronic states to be 4.58 and 4.83 eV, respectively. This result suggests that numerous rovibrational levels were located above the AlO($^2\Pi$) + H(^{2}S) and Al(^{2}P°) + OH ($^2\Pi$) dissociation limits.

Inspection of Figures 3 and 4(a) and Table 2 reveals that the $2^1A'$ and $1^1A''$ electronic states absorb strongly in the deep UV. The transition dipole moments from the ground state to these two states, which were evaluated at the CASSCF/aug-cc-pV5Z level to be 4.25 Debye, was relatively large. However, the oscillator strength that expresses the probability of absorption to these two electronic states was calculated to be 0.38 at the EOMCCSD/aug-cc-pV5Z level; the probability of this transition occurring is therefore relatively high.

Furthermore, the vertical excitation energies from the ground state to the $2^1A'$ and the $1^1A''$ states were calculated to be 5.54 and 5.59 eV, respectively. Therefore, the absorption of a photon at 5.5 eV (~220–225 nm) to these two states could lead to dissociation of the AlOH through three primary channels:

$$\mathrm{AlOH}(X^1A') + h\nu \rightarrow \mathrm{Al}(^2P^o) + \mathrm{OH}(^2\Pi) \times D_0 = 42785\ \mathrm{cm}^{-1}, \quad \text{(Ch 1)}$$

$$\mathrm{AlOH}(X^1A') + h\nu \rightarrow \mathrm{AlO}(^2\Pi) + \mathrm{H}(^2S) \times D_0 = 42819\ \mathrm{cm}^{-1}, \quad \text{(Ch 2)}$$

$$\mathrm{AlOH}(X^1A') + h\nu \rightarrow \mathrm{AlO}(^2\Sigma^+) + \mathrm{H}(^2S) \times D_0 = 63474\ \mathrm{cm}^{-1}, \quad \text{(Ch 3)}$$

Ch 1: after UV absorption, the wave packet will explore the $2^1A'$ and $1^1A''$ PESs and the molecule will undergo a large amplitude of motion. If it has sufficient energy, it can cross the barrier located at $R_{AlO} = 2$ Å and foster Al and OH in their ground electronic states (Figure 3(a)). As evident in Figure 1, the dissociation energy of the $1^1A''$ electronic state was less than 5000 cm^{-1} relative to the Al(^{2}P°) + OH ($^2\Pi$) dissociation limit. This mechanism is in good agreement with the optimized geometry

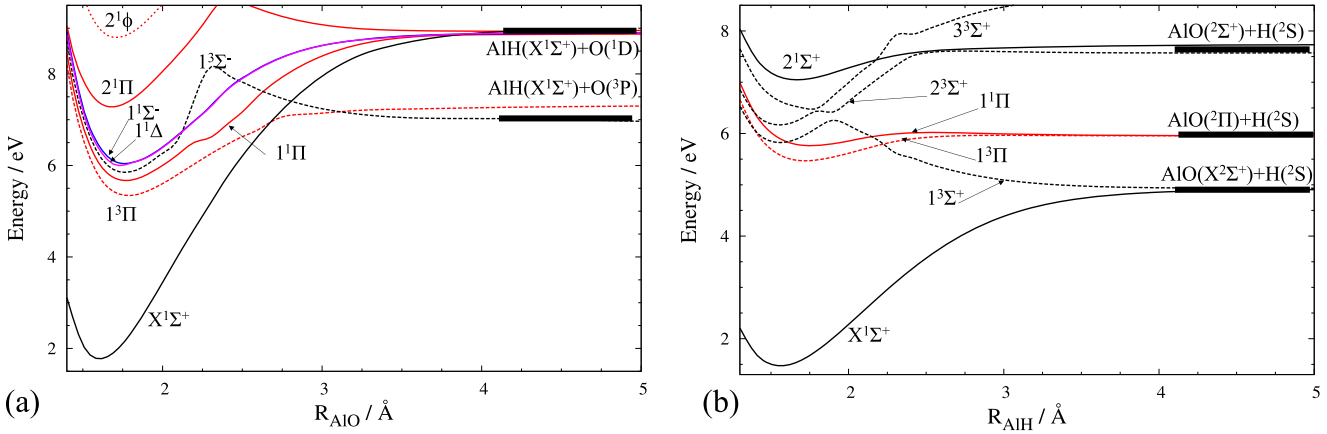

Figure 5. MRCI/aug-cc-pV5Z one-dimensional cut of the lowest singlet and triplet electronic states of HAlO along the R_{AlO} (a) and R_{AlH} (b) distances. The remaining coordinates were kept fixed at their equilibrium values. The origin of energy is the energy of AlOH in its ground electronic state.

of the $2^1A'$ and $1^1A''$ electronic states. In fact, the AlO bond length in the $2^1A'$ and $1^1A''$ states was increased by 0.053 and 0.039 Å, respectively, relative to the values in the ground electronic state. The lifetimes of these singlet states were, however, calculated to be 1.97 ns for $2^1A'$ and 1.91 ns for $1^1A''$.

The $3^1A'$ electronic state can be implicated in the photodissociatoion of AlOH because all its rovibrational levels are above the first dissociation limit Al + OH. Furthermore, the transition dipole moment $3^1A' \leftarrow X^1A'$, which was calculated to be 3.45 Debye at the CASSCF/aug-cc-pV5Z level of theory, and the oscillator strength, which was calculated at 0.30, were both relatively large. Figure 3(a) shows that the $3^1A'$ electronic state was crossed by four dissociative states, $2^1A''$, $2^3A''$, $3^3A''$, and $3^3A'$. The crossing of the $3^1A'$ state with the triplet states could, in principle, shorten the lifetime of the singlet $3^1A'$ state by spin–orbit coupling. Therefore, after UV absorption (6.36 eV at ~194 nm), the Al and OH products can occur through vibronic coupling with the $2^1A''$ electronic state or through spin–orbit coupling with the $2^3A''$, $3^3A''$, and $3^3A'$ states.

Ch 2: the other path of photodissociation is to produce AlO and H (Figure 3(b)). After UV absorption (5.5 eV at ~220–225 nm), the AlOH molecule would be excited to the $2^1A'$ or $1^1A''$ vibrational level, where it is considered to dissociate by H-atom tunneling through the barrier located at 1.21 Å and foster AlO ($^2\Pi$) + H(^{2}S) products. The optimized equilibrium geometries of these two singlets states showed that the OH bond length increased by 0.019 Å for the $2^1A'$ and by 0.016 Å for the $1^1A''$ state compared with the bond lengths in its ground electronic states. This result is in good agreement with the asymmetric stretch (ω_1), which was decreased by more than 250 cm^{-1}.

As shown in Figure 4(a), the PES of the ground electronic state along the bending angle was flat; therefore, a large variation of the bending angle corresponds to a small variation of the electronic energy. A small temperature change or infrared excitation of the vibrational mode (ν_2) could easily induce an important change in the equilibrium angle. A series of such one-dimensional cuts of the lowest singlet electronic states along the OH coordinate and at different bending angles is shown in Figure 6. These cuts give an overview of the behavior of the lowest singlet state when the bending angle changed from 120° to 180°. The evolution along the bending angle of the transition dipole moment from the ground electronic state to the lowest singlet state is shown in Figure 2. This figure shows that the transition dipole moment of $2^1A'$, $3^1A'$, and $1^1A''$ was relatively large (>3 Debye). Inspection

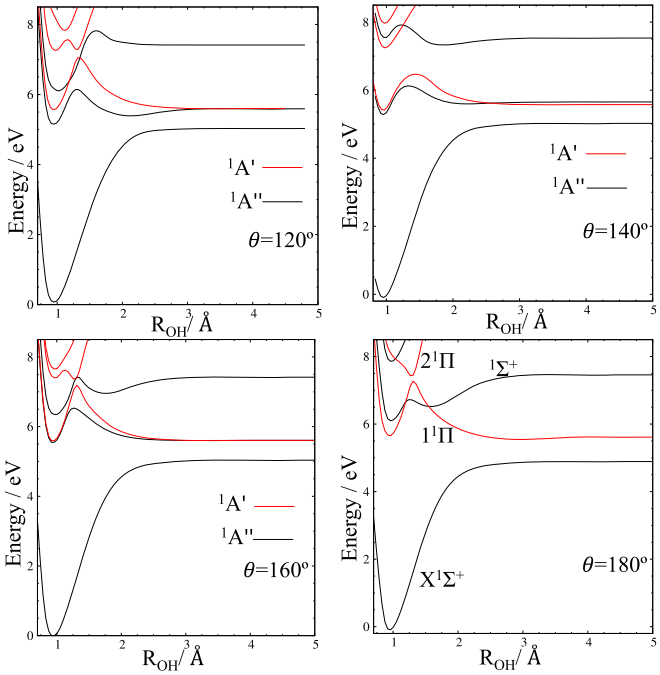

Figure 6. One-dimensional cuts of the lowest singlet state of AlOH along the R_{OH} distance and different bending angles.

of these cuts and Figure 2 shows that the $3^1A'$ electronic state can be populated after UV absorption and that the AlO($^2\Sigma^+$) + H(^{2}S) products can form (Ch 3).

For $\theta = 140°$, the $3^1A'$ state shows a low barrier at $R_{OH} = 1.3$ Å. If the molecule has sufficient energy, the wave packet will cross this low barrier and foster AlO($^2\Sigma^+$) and H(^{2}S). At linearity ($\theta = 180°$), the $3^1A'$ state correlates to the $^1\Sigma^+$ state and both $2^1A'$ and $1^1A''$ form a Renner–Teller pair and correlate to the $^1\Pi$ state. These two states, $^1\Sigma^+$ and $^1\Pi$, are crossed at $R_{OH} = 1.24$ Å and $R_{OH} = 1.57$ Å. After UV absorption, the vibrational levels of the $^1\Pi$ state can dissociate to give AlO ($^2\Pi$) through tunneling of an H atom or through vibronic coupling with the $^1\Sigma^+$ state and foster AlO($^2\Sigma^+$).

Figure 5 shows the evolution of the lowest state of HAlO along the AlH distance (Figure 5(a)) and along the AlO distance (Figure 5(b)). In these figures, the origin of energy is the energy of AlOH in its ground electronic state. Unlike the

AlOH isomer, the ground state of HAlO is linear and rigid because the bending mode ω_2 is relatively large (calculated to be 452 cm^{-1} at the MRCI+Q level). These figures show that the lowest singlet and triple electronic state are unstable with respect the first dissociation limit AlO+H (Figure 5(a)). This figure shows that several excited electronic states are stable with respect the AlH+O dissociation limit, that their minimum is located below the dissociation limit, and that they have a potential well. The evolution of the lowest singlet and triplet state along the bending angle (see Figure 4(b)) shows that several excited states are coupled by Renner–Teller coupling at linearity. When the bending angle decreases, these states split into two components, A′ and A″, in *Cs* symmetry. The optimized equilibrium geometry of the $^1\Pi$ (^{1}A′ and ^{1}A″) and $^3\Pi$ (^{1}A′ and ^{1}A″) electronic states showed them to have a bent structure (Table 2) and showed that their global minimum is located below the first dissociation limit AlO($^2\Sigma^+$)+H(^{2}S).

We now focus on the electronic spectroscopy of the HAlO isomer. We examined all allowed electronic transitions, transition dipole moments, and adiabatic and vertical excitation energies of HAlO at the MRCI+Q level. The electronic state $^1\Pi$, which is split into two components, ^{1}A′ and ^{1}A″, absorbed strongly in the near-UV. The transition dipole moment, which was calculated to be 1.87 Debye, was relatively large. The absorption of a photon to this state can easily lead to the AlO($^2\Pi$) and H(^{2}S) products. As evident in Figure 3(a), the PES of the $^1\Pi$ state was flat and the HAlO could dissociate directly to AlO($^2\Pi$) and H(^{2}S). The $^1\Pi$ electronic state was crossed by the $^3\Sigma^+$ state at $R_{AlH} = 2.19$ Å.

At this crossing, the AlO($^2\Sigma^+$) and H(^{2}S) products can also occur through spin–orbit coupling with the $^3\Sigma^+$ state. Figure 3(b) shows a high density of electronic states in the near-UV region, which favors mixing between their wavefunctions and complicates their electronic and rovibrational spectra. In this figure, all electronic states are stable with respect to the AlH+O dissociation limit and they are not crossed by any dissociative state, meaning that the photodissociation of HAlO to give AlH and O cannot occur.

4. Discussion

Close inspection of the PESs along the AlO, OH, and AlH stretching coordinates, together with the data in Table 2 and Figure 1, suggest that only Al, H, AlO, and OH products are possible through the photodissociation of AlOH and HAlO. In the case of the photodissociation of AlOH, the AlO diatomic molecule can occur only in its excited state AlO($^2\Pi$) or AlO($^2\Sigma^+$). Its production in its ground electronic state from the photodissociation of the AlOH isomer is not allowed. After the photodissociation, the diatomic AlO should return to its ground electronic state, accompanied by photon emission in the near-infrared (~2.5 μm) in the case of AlO($^2\Pi$)+H(^{2}S) (Ch 2) products and visible (blue-green) in the case of AlO($^2\Sigma^+$) +H(^{2}S) (Ch 3).

Based on our results and previous astrophysical observations, we propose that the AlO originates from the photodissociation of AlOH. The UV and visual echelle spectrograph at the large telescope does not reach the $A^2\Pi \leftarrow X^2\Sigma^+$ transition of AlO, which is located above 1.05 μm. Only the $^2\Sigma^+ \leftarrow X^2\Sigma^+$ transition was detected (Kamiński et al. 2013). Despite the high abundance of hydrogen and aluminum in VYCMa, the detection of AlH failed and the reasons for its non-detection are unclear. It has, however, been suggested to be present in VYCMa. Inspection of our PES showed that the AlH and O products cannot occur from the photodissociation of the [H, Al, O] system, which may explain why the detection of AlH has failed. At low-energy collisions, the potential energy surface suggests that AlOH formation by direct radiative association of AlO and H can occur. In fact, Figures 3(a) and (b) show that the electronic ground state and the first triplet state correlate adiabatically to the first dissociation limit AlO+H. At the CCSD(T)-F12/aug-cc-pVTZ level of theory, the optimized equilibrium geometry of the AlO–H(^{3}A′) complex show the existence of two minima corresponding to the weakly bound structure of AlOH. These two minima are bent with $R_{OH} = 3.0181$ Å, $R_{AlO} = 1.6332$ Å, and $\theta = 118.7°$ for the AlO–H(^{3}A′) complex and $R_{AlH} = 4.6561$ Å, $R_{AlO} = 1.6251$ Å, and $\theta = 151.0°$ for the H–AlO(^{3}A′) complex. These two equilibrium structures showed a real minimum on the triplet PES because all their harmonic vibrational frequencies were positive. At low temperatures, the union of AlO and H may occur through the $^3\Pi$ state and form a H–AlO(^{3}A′) van der Waals complex (Figure 5(b)). The HAlO isomer can then occur in its triplet or singlet state, followed by radiative decay to the ground electronic state.

5. Conclusion

We have reported an accurate calculation of the potential energy surfaces for the lowest singlet and triplet electronic states of AlOH and HAlO isomers. The ground electronic state of the AlOH isomer is flat, and the barrier to linearity was calculated to be 5.3 cm^{-1}. Our PES suggests that the production of AlO from AlOH is a plausible mechanism and can occur through two channels, whereas AlH and O are not allowed. Further progress can be made by combining these data with dynamics on the global PES of the first excited singlet states ^{1}A′ and ^{1}A″.

References

Adler, T. B., Knizia, G., & Werner, H. J. 2007, JChPh, 127, 221106
Hauge, R. H., Kauffman, J. W., & Margrave, J. L. 1980, J. Am. Chem. Soc., 102, 6005
Kalugina, Y. N., Buryak, I. A., Ajili, Y., et al. 2014, JChPh, 140, 234310
Kamiński, T., Schmidt, M. R., & Menten, K. M. 2013, A&A, 549, A6
Knizia, G., Adler, T. B., & Werner, H. J. 2009, JChPh, 130, 054104
Knowles, P. J., & Werner, H. J. 1985, CPL, 115, 259
Knowles, P. J., & Werner, H. J. 1988, CPL, 145, 514
Langhoff, S. R., & Davidson, E. R. 1974, IJQC, 8, 61
Li, S., Sattelmeyer, K. W., Yamaguchi, Y., & Schaefer, H. F., III 2003, JChPh, 119, 12830
Li, X., Millar, T. J., Heays, A. N., et al. 2016, A&A, 588, A4
McCabe, E. M., Smith, R. C., & Clegg, R. E. S. 1979, Natur, 281, 263
Michels, H. H. 1972, JChPh, 56, 665
Mizushima, M. 1972, PhRvA, 5, 143
Parsons, S. G., Marsh, T. R., Copperwheat, C. M., et al. 2010, MNRAS, 407, 2362
Pilgrim, J. S., Robbins, D. L., & Duncan, M. A. 1993, CPL, 202, 203
Pulliam, R. L., Savage, C., Agúndez, M., et al. 2010, ApJL, 725, L181
Rosenwaks, S., Steele, R. E., & Broida, H. P. 1975, JChPh, 63, 1963
Sghaier, O., Linguerri, R., Al Mogren, M. M., Francisco, J. S., & Hochlaf, M. 2016, ApJ, 826, 163
Tenenbaum, E. D., & Ziurys, L. M. 2009, ApJL, 694, L59
Tenenbaum, E. D., & Ziurys, L. M. 2010, ApJL, 712, L93
Werner, H.-J. 2015, MOLPRO, version 2015.1, A Package of ab initio Programs, http://www.molpro.net
Werner, H. J., Adler, T. B., & Manby, F. R. 2007, JChPh, 126, 164102
Werner, H. J., & Knowles, P. J. 1985, JChPh, 82, 5053
Werner, H. J., & Knowles, P. J. 1988, JChPh, 89, 5803
Ziurys, L. M. 2006, PNAS, 103, 12274
Ziurys, L. M., Apponi, A. J., Guélin, M., & Cernicharo, J. 1995, ApJL, 445, L47
Ziurys, L. M., Savage, C., Highberger, J. L., et al. 2001, ApJL, 564, L45